Dalton Transactions

RSC Publishing

PAPER

New tris-3,4-HOPO lanthanide complexes as potential imaging probes: complex stability and magnetic properties†

Cite this: *Dalton Trans.*, 2013, **42**, 6046

Ana C. Mendonça,[a] André F. Martins,[b,c,d] Andrea Melchior,[e] Sérgio M. Marques,[a] Sílvia Chaves,[a] Sandrine Villette,[d] Stéphane Petoud,[d] Pier Luigi Zanonato,[f] Marilena Tolazzi,[e] Célia S. Bonnet,[d] Éva Tóth,[d] Plinio Di Bernardo,[f] Carlos F. G. C. Geraldes[b,c,g] and M. Amélia Santos*[a]

Received 24th September 2012,
Accepted 29th November 2012

DOI: 10.1039/c2dt32237d

www.rsc.org/dalton

There is a growing interest in the development of new medical diagnostic tools with higher sensibility and less damage for the patient body, namely on imaging reporters for the management of diseases and optimization of treatment strategies. This article examines the properties of a new class of lanthanide complexes with a tripodal tris-3-hydroxy-4-pyridinone (tris-3,4-HOPO) ligand – $NTP(PrHP)_3$. Among the studies herein performed, major relevance is given to the thermodynamic stability of the complexes with a series of Ln^{3+} ions (Ln = La, Pr, Gd, Er, Lu) and to the magnetic relaxation properties of the Gd^{3+} complex. This hexadentate ligand enables the formation of (1 : 1) Ln^{3+} complexes with high thermodynamic stability following the usual trend, while the Gd-chelates show improved relaxivity (higher hydration number), as compared with the commercially available Gd-based contrast agents (CAs); transmetallation of the Gd^{3+}–L complex with Zn^{2+} proved to be thermodynamically and kinetically disfavored. Therefore, $NTP(PrHP)_3$ emerges as part of a recently proposed new generation of CAs with prospective imaging sensibility gains.

Introduction

Lanthanide complexes have been the object of intensive studies over the past two decades due to the emergence of new classes of metallodrugs as bioactive probes with potential magnetic resonance and luminescence imaging applications in biology or in modern diagnostic medicine, as non-invasive and non-ionizing radiation techniques with proved clinical ability.[1,2]

Magnetic resonance imaging (MRI) has become a particularly effective tool in diagnostics but, in specific cases, the administration of paramagnetic Ln^{3+} complexes as contrast agents (CAs) largely contributes to the success of this imaging modality.[3] Gd^{3+} complexes have been found to be the most suitable CAs for MRI due to the high paramagnetism ($4f^7$) and long electron spin relaxation times of the metal ion.[3c] However, the high toxicity of the free lanthanide ions determines their administration as chelates with high thermodynamic and kinetic stability.[4] The efficacy of a CA is measured by its ability to selectively enhance the relaxation of water protons in different tissues. This is expressed by its relaxivity (r_i, i = 1, 2), which represents the relaxation rate enhancement of water protons in solutions containing the CA at 1 mM concentration. Further properties of these agents are of paramount importance to improve imaging sensibility, such as the number of inner-sphere coordination water molecules, their exchange rate with bulk solution, the rotational and translational diffusion of the CA, as well as the optimal delivery features of the metal complexes to guarantee a high concentration of the CA at the target tissue.[5–7]

The commercially available CAs employ polyamino-carboxylate ligands to coordinate the Gd^{3+} cation. Some of these chelators are linear (*e.g.* diethylenetriamine-pentaacetic acid (H_5DPTA)), while others are macrocyclic (*e.g.* 1,4,7,10-

[a]*Centro de Química Estrutural, Instituto Superior Técnico, Universidade Técnica de Lisboa, Av. Rovisco Pais 1, 1049-001 Lisboa, Portugal. E-mail: masantos@ist.utl.pt; Fax: +00351-218464455; Tel: +00351-218419273*
[b]*Department of Life Sciences, Faculty of Science and Technology, University of Coimbra, P.O. Box 3046, 3001-401 Coimbra, Portugal*
[c]*Center of Neurosciences and Cell Biology, Largo Marquês de Pombal, University of Coimbra, Portugal*
[d]*Centre de Biophysique Moléculaire, CNRS, Rue Charles Sadron, 45071 Orléans, France*
[e]*Dipartimento di Chimica Fisica e Ambiente, Università di Udine, Via del Cotonificio 108, 33100 Udine, Italy*
[f]*Dipartimento di Scienze Chimiche, Università di Padova, Via Marzolo 1, 35131 Padova, Italy*
[g]*Coimbra Chemistry Center, Rua Larga, University of Coimbra, 3004-535 Coimbra, Portugal*
†Electronic supplementary information (ESI) available. See DOI: 10.1039/c2dt32237d

tetraazacyclododecane-1,4,7,10-tetraacetic acid (H_4DOTA)). Since they are octadentate ligands, only one coordination site is open for one inner-sphere water molecule. To increase the relaxivity of these types of complexes a great deal of research has focused on enhancing the hydration number or on slowing down the molecular tumbling, though the results obtained are still far from ideal.[7] This challenging goal leads to the study of another family of Ln^{3+} complexes, based on the tripodal hydroxypyridinone (HOPO).[8,9] Three of these *O*,*O*-donor chelating units (3,2-HOPOs and 1,2-HOPOs) were appended to anchoring scaffolds (*e.g.* tris(2-aminoethyl)amine (TREN) and triazacyclononane (TACN))[10] to provide hexadentate coordination to the oxophilic Gd^{3+} cation and formation of very stable complexes, while still leaving two open water coordination sites in its overall eight coordinated complex. Some of these novel Gd^{3+} complexes presented higher stability (pGd = 16–21) than the commercial agents (pGd = 19.2 for DPTA and 20.4 for DOTA)[9] and attained higher relaxivity, mainly due to their higher hydration number (q = 2) and slower tumbling rates.[11]

On the other hand, several Ln^{3+} complexes exhibit intense luminescence and thus visible (VIS) emitting (*e.g.* Eu^{3+} and Tb^{3+}) or near infrared (NIR) Ln^{3+} emitting (Ln = Sm, Dy, Pr, Ho, Yb, Nd, Er) complexes have recently received most attention, due to their application in biotechnology and medicinal chemistry (optical imaging).[2] Two recent reviews have highlighted the most important progress in emissive lanthanide complexes, namely in complexes with DOTA[12] or HOPO-based[13] coordinating frameworks. In contrast to the MRI probes, the degree of hydration of the luminescent probes should be minimized to avoid the loss of excited state energy (nonradioactive deactivation processes-quenching) from the Ln^{3+} ion to vibrational energy of bound (or nearby) OH oscillators.

Given the recognized growing interest in the development of new imaging probes for biomedical applications, the high relaxivity demonstrated for Gd^{3+} complexes with 1,2-HOPOs and 2,3-HOPOs[8,11] together with the discovery of highly efficient sensitization of Tb^{3+} and Eu^{3+} with 1,2-HOPO-based chromophores,[13,14] we have decided to investigate a similar oxo hexadentate ligand with three 3-hydroxy-4-pyridinone (3,4-HOPO) chelating units attached to the anchoring scaffold nitrilopropionic acid (NTA), the tripodal tris-3,4-HOPO = NTP(PrHP)$_3$ (see Fig. 1). Since NTP(PrHP)$_3$ already evidenced high capacity for formation of stable complexes with *hard* Lewis acid M^{3+} ions (M = Fe, Al, Ga; pFe = 29.4; pAl = 22.4; pGa = 27.5)[15,16] in aqueous solution, a similar behavior could be anticipated for Ln^{3+} cations, because, especially at the end of the series (lanthanide contraction),[17] they have a high positive surface charge density and behave as *hard* Lewis acids. On the other hand, the corresponding ^{67}Ga complex with this ligand also demonstrated high *in vivo* stability and good excretion profiles.[16] Furthermore, the investigation on the thermodynamic properties of the Zn^{2+} complex with NTP(PrHP)$_3$ also appeared of interest, as this ion can compete with Ln^{3+} ions for this ligand causing the release of the toxic free lanthanide *in vivo*.

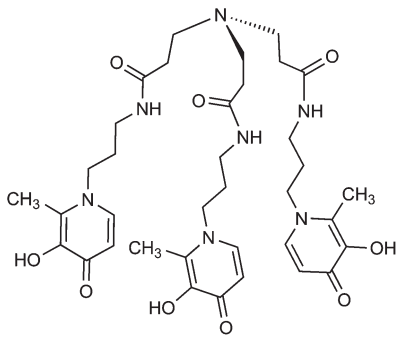

Fig. 1 Molecular structure of the tris-3,4-HOPO ligand (L = NTP(PrHP)$_3$).

This paper is specially focused on solution studies to evaluate (i) the thermodynamic stability of a set of lanthanide complexes with a tris-3,4-HOPO ligand, by potentiometry and spectrophotometry, besides a brief study on the selectivity of the ligand for Gd^{3+} over Zn^{2+} to avoid *in vivo* demetallation of the Gd^{3+} complex and appearance of nephrogenic systemic fibrosis (NSF),[17] (ii) the water exchange rate and relaxometric properties of the GdL complex from ^{1}H NMRD (nuclear magnetic relaxation dispersion) data and (iii) the luminescence lifetime properties of a series of Ln–L complexes. Complementary DFT theoretical calculations on the GdL complex are also carried out to aid the rationalization of the experimental results.

2. Results

2.1. Thermodynamics and coordination of Ln–L complexes

2.1.1. Protonation studies. The acid–base properties of NTP(PrHP)$_3$, at 25 °C and in 0.1 mol dm^{-3} KCl, have already been reported and the specific donor sites involved in the protonation/deprotonation reactions determined on the basis of potentiometric, spectrophotometric and ^{1}H NMR titrations.[15,16] Herein, potentiometric and spectrophotometric titrations of the ligand were carried out, under the same experimental conditions, in order to introduce the obtained data on the model for the lanthanide complexation.

The potentiometric titration curve of the ligand alone is reported in Fig. 2 and in Table 1 the protonation constants obtained from the best fitting of the present experimental data are given, all in fairly-good agreement with those previously obtained.[15]

The spectrophotometric titration of the fully protonated ligand with a strong base solution (Fig. S1†) shows that in the range of pH 0.98–2.36, two absorbance maxima (λ_{max} = 280 and 244 nm) are present and only slightly modified by increasing pH (Fig. S1-a†). In the range of pH = 3.19–8.60, an increase of absorbance at 280 nm occurs and a new maximum appears at 304 nm. Above pH 8.60 the absorbance of the band at 280 nm decreases while that at 304 nm increases (see Fig. S1-b†).

A comparison of the absorbance changes at λ_{max} = 304, 280 and 244 nm with the ligand speciation at different pH values

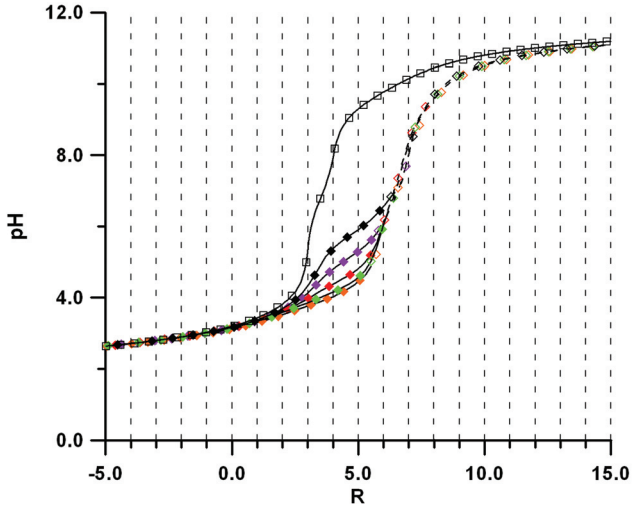

Fig. 2 Titration curves for the ligand alone (□, C_L 0.585 mmol dm^{-3}) and in the presence of lanthanide ions in the 1 : 1 molar ratio: ◆ C_{La} 0.375; ◆ C_{Pr} 0.369; ◆ C_{Gd} 0.371; ◆ C_{Er} 0.370; ◆ C_{Lu}. 0.377 mmol dm^{-3}. Only some of the experimental points are reported in the plot. Full lines, calculated with the stability constants of Tables 1 and 2. Dashed lines, eye guides connecting the experimental points (empty symbols) collected in the presence of precipitate.

Table 1 Overall and stepwise protonation constants of the ligand **L** (LH_j), at 25 °C and I = 0.1 M KCl

Reaction	j	$\log \beta_j \pm \sigma$	$\log K_j$	$\log K_i^a$
$L^{3-} + H^+ \rightleftarrows HL^{2-}$	1	10.06 ± 0.03	10.06	9.95(1)
$L^{3-} + 2H^+ \rightleftarrows H_2L^-$	2	19.75 ± 0.02	9.69	9.84(1)
$L^{3-} + 3H^+ \rightleftarrows H_3L$	3	28.93 ± 0.02	9.18	9.09(8)
$L^{3-} + 4H^+ \rightleftarrows H_4L^+$	4	35.72 ± 0.03	6.81	6.77(1)
$L^{3-} + 5H^+ \rightleftarrows H_5L^{2+}$	5	39.46 ± 0.04	3.74	3.81(1)
$L^{3-} + 6\ H^+ \rightleftarrows H_6L^{3+}$	6	42.51 ± 0.04	3.05	3.14(1)
$L^{3-} + 7H^+ \rightleftarrows H_7L^{4+}$	7	44.38 ± 0.17	1.87	2.76(2)

Notes: The water ionization constant (pK_w) is 13.78 ± 0.01 in aqueous solution under the conditions employed. [a] From ref. 16.

in Fig. 3 allows correlation of the different protonation sites with their characteristic absorptions in the spectra.

The large spectral changes at 280 nm occurring at pH < 3.5 can be assigned to the deprotonation of pyridinium nitrogens, whereas the changes of the absorption at 304 nm, observed after pH 8–9, to the deprotonation of pyridinone hydroxyl groups. This is in agreement with previous NMR results.[15]

The distribution plot in Fig. 3 shows that in the pH range 4–6 and 7.7–8.5, the most abundant species are H_4L and H_3L, respectively. H_4L is the $[NTP(PrHP)_3H]^+$ species whose protonated sites are three hydroxyl groups and the apical nitrogen. At physiological conditions (pH = 7.4), the solution is a mixture of ~20% H_4L and ~80% H_3L. The very small absorbance change between pH 3.5 and 8.6 agrees with the already suggested deprotonation of the apical nitrogen in this pH range.[15] According to the above considerations, data in Fig. 3 indicate that the absorption at ~280 nm is characteristic of both H_4L and H_3L, whereas the absorption at ~304 nm corresponds to the deprotonated-ligand forms (H_2L, HL and L).

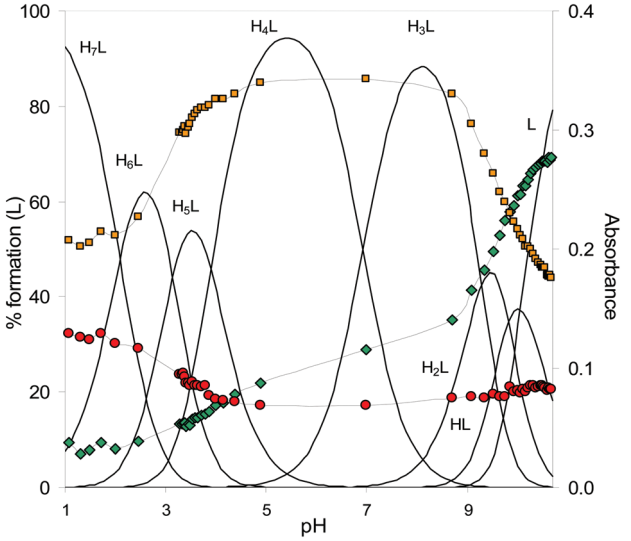

Fig. 3 Distribution species diagram of L (NTP(PrHP)$_3$) together with the absorbance values at 304 (green), 280 (orange) and 244 nm (red) (C_L = 1.3 × 10^{-5} mol dm^{-3}). See also Fig. S1.†

2.1.2. Lanthanide(III) complexation. Some examples of the potentiometric titration curves obtained for 1 : 1 Ln^{3+}–L systems are reported in Fig. 2 which shows that the complex formation already occurs from pH 3.0–3.5. All the solutions containing the metal ions are much more acidic than those with the ligand alone, and all the titration curves have similar profiles with a coalescence point at $R \sim 7$,‡ suggesting the formation of complexes with the same type of stoichiometry, although with different metal–ligand affinity. The formation of a solid phase was noted when R is close to 7 (see dashed curves and empty symbols), which can be attributed to the formation of the neutral 1 : 1 complex, ML. The stoichiometry of the complexes and the overall stability constants yielding the best fit of the pH-metric titration curves are shown in Table 2, which indicates that the lanthanide ions can bind to the ligand with formation of both 1 : 1 and 1 : 2 complexes protonated at different degrees.

It is noticeable that, differently from the complexation model found for Group III metal complexes,[15,16] the equilibrium model found for the lanthanide complexation admits two extra protonated complex species (MH_4L and MH_2L), thus suggesting an apparent lack of cooperativity between the binding of the hydroxypyridinone (HP) moieties to the metal ion and the release of both the hydroxyl and the pyridinium protons.

The stability constants of the metal complexes are much higher than those of singly-charged oxygen donors[18] and are correlated with the reciprocal of the ionic radius of the

‡$R = n'_{OH}/n_L$ or n'_{OH}/n_{Ln3+} where $n'_{OH} = n_{OH} - (n_{H+} - 7n_L)$: *i.e.* the difference between the number of moles of base added and the excess moles of mineral acid corrected for the full protonation of the ligand (H_7L^{4-}). Therefore R = 0 when the excess acid is completely neutralized and the ligand is formally heptaprotonated.

Table 2 Stability constants for formation of Ln^{3+}–L complexes, $M_1H_hL_l$ (M = La, Pr, Gd, Er, Lu) at 25 °C, I = 0.1 M KCl, and estimated $1/R_{CN}$ values (R = ionic radii for coordination number (CN) 9)[a]

Ln^{3+}	$1/R_{CN=9}$	log β_{151}	log β_{141}	log β_{131}	log β_{121}	log β_{111}	log β_{152}	log β_{132}
La	0.822	42.8 ± 0.1	39.46 ± 0.06	34.70 ± 0.04	29.0 ± 0.3	22.86 ± 0.04	62.63 ± 0.06	49.2 ± 0.1
Pr	0.848	43.7 ± 0.1	40.36 ± 0.07	35.99 ± 0.07	30.72 ± 0.06	25.29 ± 0.06	65.04 ± 0.09	51.6 ± 0.2
Gd	0.903	42.8 ± 0.2	39.46 ± 0.08	35.69 ± 0.08	31.16 ± 0.06	26.35 ± 0.05	65.3 ± 0.2	52.3 ± 0.2
Er	0.942	42.3 ± 0.3	39.35 ± 0.06	35.45 ± 0.1	31.70 ± 0.04	26.77 ± 0.03	66.1 ± 0.2	52.9 ± 0.2
Lu	0.969	43.34 ± 0.04	39.86 ± 0.03	36.12 ± 0.05	32.35 ± 0.02	27.53 ± 0.02	67.53 ± 0.04	54.4 ± 0.1

[a] From ref. 20.

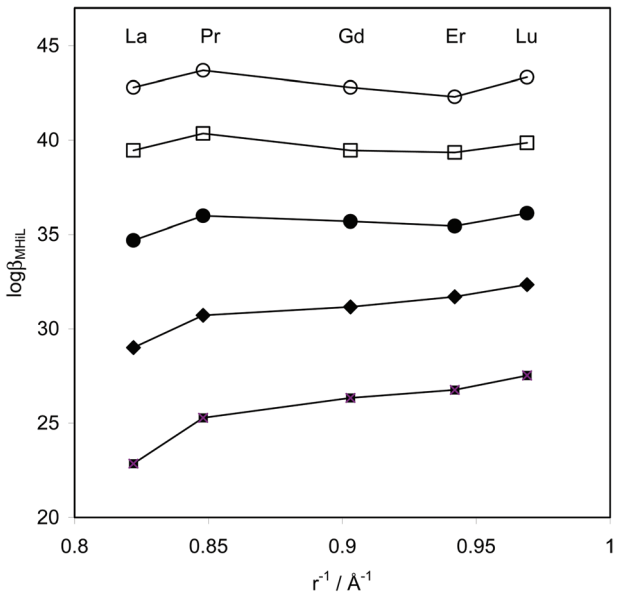

Fig. 4 Graphical representation of log β_{MH_iL}, i = 1–5 as a function of r^{-1} (r = ionic radius) for the Ln^{3+} ions (Ln = La, Pr, Gd, Er, Lu): (■) log β_{MHL}; (◆) log β_{MH_2L}; (●) log β_{MH_3L}; (□) log β_{MH_4L}; (○) log β_{MH_5L}.

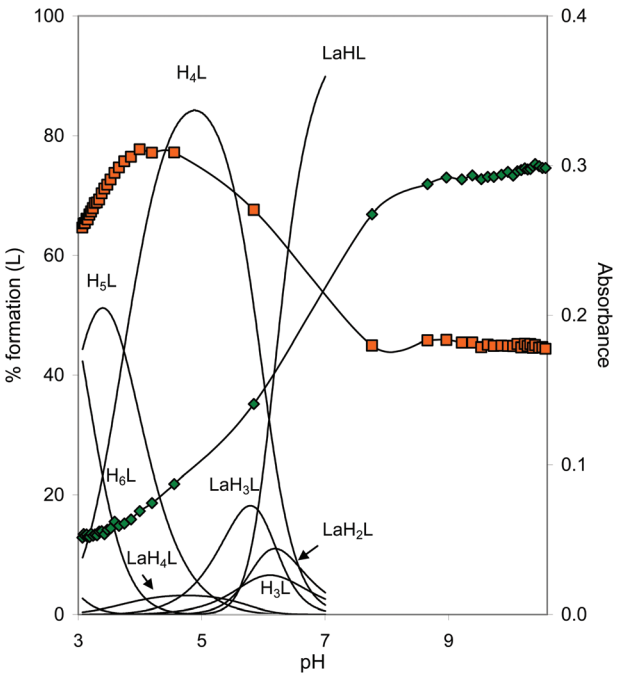

Fig. 5 Speciation diagrams for the La^{3+}–L system (pH 3–7) together with the absorbance changes at 280 nm (orange) and 306 nm (green) (C_L = 1.3 × 10^{-5} mol dm^{-3}, C_L/C_{La} = 1.01). The speciation plot was limited to pH ~ 7 because of the precipitation occurring in the concentration range used for potentiometric titrations.

different ions, following a *quasi*-parallel wavy trend (Fig. 4). In particular, the stability constants for the formation of MH_2L and MHL complexes increase by about a factor of 10^4 on going from La^{3+} to Lu^{3+}. This behaviour was previously observed for the complexation of other tripodal ligands,[19,20] and it is expected on the basis of the harder acid character of heavier Ln^{3+} cations, as a consequence of the well known *lanthanide contraction*.[20,21] The increase of log β_{MH_iL} on going from La^{3+} to Lu^{3+} shows that the complex stabilities are determined by a stronger electrostatic interaction with Ln^{3+} ions with smaller ionic radii (Fig. 4). However, the lanthanide–ligand interaction is modulated also by the increase of the steric strain of the ligand which has to wrap around smaller cations. The compensation of these two effects is reflected in the observed wavy trend of the log β_{MH_iL} values.[22,23]

Spectrophotometric titrations were carried out to help the identification of the specific donor groups of the ligand involved in the metal chelation. The marked differences§ of the spectra in the absence (Fig. S1-b†) and in the presence of the metal ion (Fig. S2†) can be attributed to the formation of LaH_nL species (see the speciation plot in Fig. 5). The spectral variations continue above pH 7, where the potentiometric titrations were interrupted due to the formation of a solid phase (Fig. 2). Therefore the speciation plot was limited to pH ~ 7. However, spectrophotometric data were collected up to pH ~ 11 because, in that case, the lanthanide concentration in solution was about one order of magnitude lower than that used in the potentiometric experiments and formation of solid phases was never observed.

A comparison between the speciation plot and the absorbance changes in Fig. 5 provides useful information about the sequence of deprotonation of the complexes. The largest absorbance changes in this figure occur in the range of pH 6–8, where reasonably the deprotonation of the

§ From pH ~ 4.2 with a net increase of the band at 306 nm and a concomitant decrease of the band at 280 nm.

spectroscopically most active ligand sites, the HP moieties, takes place; whereas after pH = 8, the spectra remain almost unchanged suggesting that in that pH region LaHL loses its apical proton, spectroscopically silent. This proton is less acidic than in H_4L, which deprotonates at lower pH values (Fig. 3). A reasonable explanation for this is given by theoretical calculations which show that in the optimized structures of the LnHL complexes the lanthanide ion forces the arms of this flexible ligand to a relatively rigid structure where the apical proton (both in "*in*" and "*out*" isomers) can form intramolecular hydrogen bonds either with the carbonyl group of one arm (Fig. 6a) or with an oxygen of the hydroxypyridinone moiety (Fig. 6b).

The affinity of the ligand towards Zn^{2+} was also evaluated in order to gain some insight into the selectivity of the ligand for Gd^{3+} relative to Zn^{2+}. Preliminary potentiometric studies and data analysis evidenced that formation of zinc complexes (ZnH_iL) begins above pH = 2 with different degrees of protonation (i = 1–5). The two mononuclear species ZnH_2L and ZnHL present maximum abundance around pH 6 and 8, respectively. Apparently there is also a minor formation of the trinuclear species Zn_3L_2 above pH 7. The log values of the overall stability constants for ZnHL and ZnH_2L are 22.11 and 29.26, respectively, and the calculated pZn at pH = 7.4 ($C_M = 10^{-6}$ M and $C_L = 10^{-5}$ M) is 9.1 (Table S1†). The pLn^{3+} values at the same pH and metal–ligand concentrations range from 9.75 to 14.71, for Ln = La and Lu, respectively. Therefore, the possibility of transmetallation of the Gd^{3+}–L complex with Zn^{2+} is thermodynamically disfavored.

2.2. Molecular modeling

Since our efforts to obtain good crystalline samples of the Ln^{3+}–L complex for X-ray diffraction were unsuccessful, DFT calculations were carried out to optimize in vacuum the structures of two isomers of the $[Ln(HL)(H_2O)_2]^+$ (Ln = La, Gd, Lu) complexes: (a) with the apical H directed outside the cavity of the tripod ("out" conformation, Fig. 6a), (b) with the apical H directed inside the cavity of the tripod ("in" conformation, Fig. 6b). The energies of the complexes were then calculated in the presence of implicit water (PCM) using the gas-phase equilibrium geometry.

Only two experimental structures for the Gd and La complexes with a similar tripodal contrast agent (TREN-Me-3,2-HOPO, with TREN (tris(2-aminoethyl)amine) backbone) are available in the literature.[24,25] It is of interest to note that in both complexes the first coordination sphere of the lanthanides is occupied by the ligand and two water/solvent molecules.

The calculated Gd–O (ligand) bond distances (Table 3) are in good agreement with the experimental data (averaged exp. 2.38(3) Å) while the Gd–O (water) bond distance (exp. 2.44(1) Å) is overestimated.[24] Also the La–O distances are in good agreement with the published crystal structure (exp. 2.50(4) Å)[25] and again the La–O (water) results are somewhat overestimated by our calculations (exp. 2.49 Å).[25] This discrepancy between calculated and experimental Ln–O (water) bond distances may be due to the distinct flexibility and steric requirements of the two ligands which are able to encapsulate the lanthanide ion to a different extent. The Ln–O (ligand)

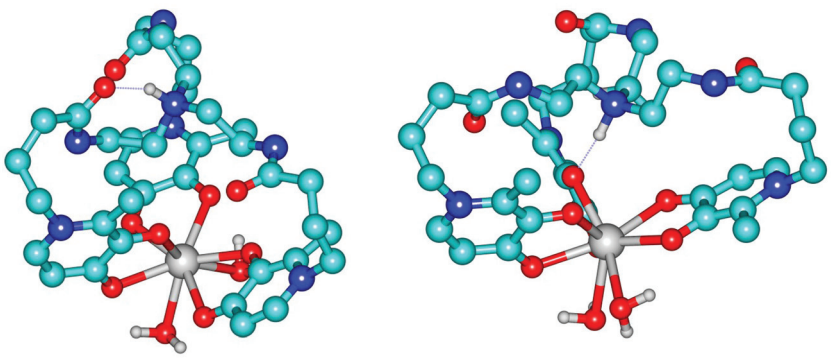

Fig. 6 DFT optimized structures of the $[Gd(HL)(H_2O)_2]^+$ complexes: (a) "out" conformation, (b) "in" conformation. Intramolecular hydrogen bonds are evidenced with a dotted line; non-ionizable H atoms are omitted.

Table 3 Some calculated properties for the $[Ln(HL)(H_2O)_2]^+$ complexes. The ΔE values are in kcal mol^{-1}, r_{Ln-Ox} bond distances (Å) reported as average values with standard deviation in parenthesis, lanthanide partial charge (q_{Ln}) is in electrons

	$\Delta E_{out\text{-}in}{}^{gas}$	$\Delta E_{out\text{-}in}{}^{water}$	$\Delta E_{out\text{-}in}{}^{def}$	$\Delta E^{def,Ln}$ out, in	q_{Ln}	$r_{Ln\text{-}OW}$ out, in	$r_{Ln\text{–}O\ ligand}$ out, in
$[La(HL)(H_2O)_2]^+$	−2.5	−4.4	12.4	0.0	1.197	2.69(4), 2.69(1)	2.52(6), 2.50(5)
$[Gd(HL)(H_2O)_2]^+$	−1.4	−2.9	13.0	8.5, 9.1	1.151	2.58(7), 2.61(1)	2.42(8), 2.40(6)
$[Lu(HL)(H_2O)_2]^+$	−1.7	−3.2	14.5	19.8, 21.9	1.093	2.5(1), 2.46(1)	2.31(4), 2.31(4)

bond distances decrease from La to Lu (Table 3) indicating a stronger cation–ligand interaction with the increase of the atomic number. Also the decrease of the Mulliken charge of the lanthanides (Table 3) is consistent with a strong electrostatic interaction with the donor atoms of the ligand. Even if indirectly, this stronger cation–ligand interaction is reflected in the stability constants of the $[LnHL]^+$ complexes, which increase by more than 4 orders of magnitude on going from La to Lu. In Fig. 6 it is also evident that the apical proton is able to form intramolecular hydrogen bonds (dotted lines) both in the "in" and "out" conformation.¶

In Table 3 the difference in energy between the "out" and "in" conformers ($\Delta E_{\text{out-in}} = E_{\text{out}} - E_{\text{in}}$) evidences that for all lanthanides the "out" conformation is more stable both in vacuum and especially in PCM water. Additionally, it can be seen that this stabilization decreases on going from La to Lu. Also from previous DFT calculations for the corresponding ferric complex the "out" conformation appeared slightly more stable than the "in" conformation.[15] However, the "in" conformation was found for the X-ray structure of the ferric complex with another tripodal hexadentate 3-hydroxy-2-pyridinone (FeCP130).[26] It is also interesting to note in Table 3 that the difference of the energy of the ligand alone at the coordinates in the optimized complexes in gas-phase ($\Delta E_{\text{out-in}}^{\text{def}} = E_{\text{ligand,out}} - E_{\text{ligand,in}}$) is always positive: this indicates that the energetic cost to adapt the "out" conformer to the coordinates of the optimized complex is higher. The fact that $\Delta E_{\text{out-in}}$ (Table 3) is more favorable for the "out" complex suggests that the higher strain energy of the ligand in the "out" conformation ($\Delta E_{\text{out-in}}^{\text{def}}$ always positive) is compensated by a better interaction with the lanthanide ion. Additionally, the gas-phase energy of the ligand in the Gd^{3+} and Lu^{3+} complexes relative to that in the La^{3+} complex ($\Delta E^{\text{def,Ln}} = E_{\text{ligand}}^{\text{Ln}} - E_{\text{ligand}}^{\text{La}}$) clearly increases on going from La^{3+} to Lu^{3+} both for the "in" and the "out" isomers. This agrees with the fact that the heavier lanthanides with smaller ionic radius induce a higher strain in the ligand structure.[20] Therefore the results of these energy terms ($\Delta E_{\text{out-in}}^{\text{def}}$, $\Delta E_{\text{out-in}}^{\text{def,Ln}}$) suggest that the strength of the binding of the lanthanide ion is mostly determined by the electrostatic interaction between the ion and the donor atoms rather than steric factors, as also indicated by the bond distances and the atomic charge (Table 3).

2.3. Water exchange rate and relaxometric properties of GdL

In order to assess the parameters characterizing water exchange on GdL, we have measured variable temperature transverse ^{17}O NMR relaxation rates and chemical shifts at 11.7 T in aqueous solutions of the complex. The hydration number of GdL was assumed to be $q = 2$, analogously to similar HOPO-type complexes.[8] This assumption is in full accordance with the experimental ^{17}O chemical shifts and with the molecular modelling results. Although the quality of the chemical shift data is relatively poor due to the limited solubility, and thus low concentration of the complex in the ^{17}O NMR sample, they prove the bishydrated nature of GdL.

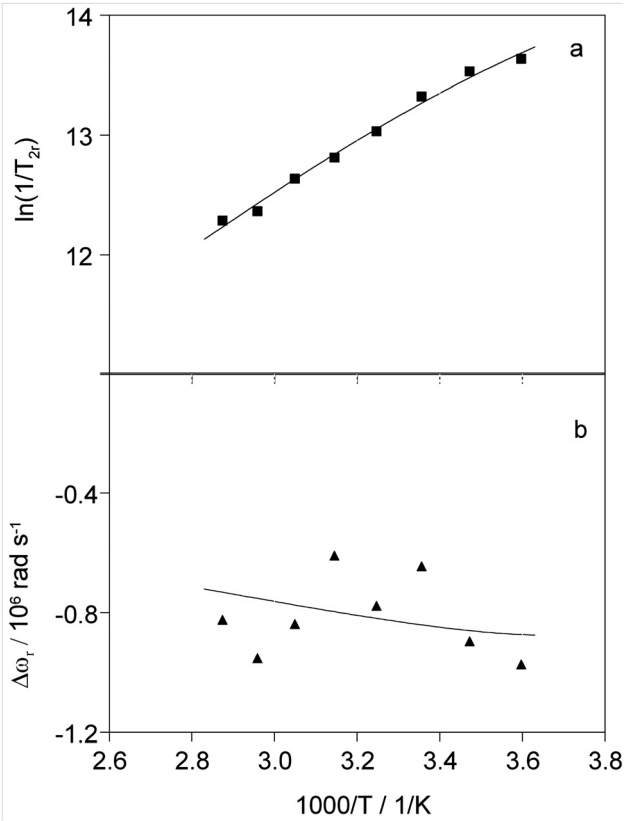

Fig. 7 Reduced transverse ^{17}O relaxation rates (a) and ^{17}O chemical shifts (b) of a GdL solution at 11.75 T, pH = 6.5. The solid lines represent the least-squares fit as explained in the text.

The reduced ^{17}O transverse relaxation rates, $1/T_{2r}$, increase with decreasing temperature characteristic of a fast exchange region (Fig. 7). In the fast exchange regime, the reduced transverse relaxation rate is defined by the transverse relaxation rate of the bound water oxygen, $1/T_{2m}$, which is in turn influenced by the water exchange rate, k_{ex}, the longitudinal electronic relaxation rate, $1/T_{1e}$, and the scalar coupling constant, $A/\hbar$. The reduced ^{17}O chemical shifts are determined by $A/\hbar$. The experimental ^{17}O NMR data have been fitted to the Solomon–Bloembergen–Morgan theory of paramagnetic relaxation (equations given in the ESI†). The following parameters have been adjusted: the water exchange rate, k_{ex}^{298}, the activation entropy, $\Delta S^{\ddagger}$, and the activation enthalpy, $\Delta H^{\ddagger}$, for water exchange, the scalar coupling constant, $A/\hbar$, and the parameters characterizing the electron spin relaxation, such as the correlation time for the modulation of the zero-field-splitting, τ_v^{298}, its activation energy, E_v, and the mean-square zero-field-splitting energy, Δ^2. The parameters calculated are shown in Table 4. For the parameters characterizing electron spin relaxation, we calculated $\tau_v^{298} = 4.1 \pm 0.5$ ps and $\Delta^2 = (0.8 \pm 0.1) \times 10^{20}$ s^{-2}, while E_v was fixed to 1 kJ mol^{-1}. We should note that the contribution of the electron spin relaxation is relatively low

¶The H···O distance is 1.696 Å and 1.685 Å from the oxygen of the HP moiety ("in") and from amide oxygen ("out"), respectively.

Table 4 Parameters obtained from the analysis of ^{17}O NMR and NMRD data

Parameter	GdL	Gd[TREN-Me-3,2-HOPOTAM][a]
$k_{ex}^{298}/10^7$ s^{-1} [b]	6.5 ± 0.6	9.1
$\Delta H^{\ddagger}$ kJ mol^{-1} [b]	18.5 ± 0.8	7.0
$\Delta S^{\ddagger}$ J mol^{-1} K^{-1} [b]	−33 ± 3	—
$A/\hbar/10^6$ rad s^{-1} [b]	−3.2 ± 0.3	−3.6
τ_R^{298}/ps [c]	127 ± 11	125
E_r/kJ mol^{-1} [c]	12.0 ± 0.9	—
τ_v^{298}/ps [c]	14 ± 2	18
$\Delta^2/10^{20}$ s^{-2} [c]	3.1 ± 0.1	1.1
E_v/kJ mol^{-1} [c]	1.0	—

[a] Ref. 25. [b] Obtained from ^{17}O NMR data. [c] Obtained from NMRD data, see text.

with respect to the water exchange rate ($1/T_{1e}$ contributes 9–35% to the correlation time that governs T_2 relaxation, $1/\tau_c = k_{ex} + 1/T_{1e}$). Therefore the parameters for electron spin relaxation are not well-determined. On the other hand, the value of the water exchange rate is reliable. This value, $k_{ex}^{298} = (6.5 \pm 0.6) \times 10^7$ s^{-1}, is similar to or slightly lower than those reported by Raymond *et al.* for their Gd–HOPO complexes (~10^8 s^{-1}),[8] and considerably higher than the water exchange rates of commercial contrast agents (0.4–4) × 10^6 s^{-1}. The negative activation entropy, $\Delta S^{\ddagger} = -33 \pm 5$ J mol^{-1} K^{-1}, points to the associative character of the water exchange mechanism, in accordance with the octa-coordinated nature of the GdL complex. Indeed, the typical coordination numbers of Gd^{3+} in solution are 8 and 9, consequently, eight-coordinate complexes undergo associatively activated water exchange, while nine-coordinate complexes are characterized by dissociatively activated water exchange. The associative water exchange mechanism has been directly evidenced by the negative activation volume ($\Delta V^{\ddagger} = -5$ cm^3 mol^{-1}) obtained from variable pressure ^{17}O NMR measurements for Gd-TREN-bis(6-Me-HOPO)-(TAM-TRI).[27]

The magnetic field dependence of the longitudinal water proton relaxivities (r_1) was measured by ^1H nuclear magnetic relaxation dispersion (NMRD) with the objective of determining the parameters that describe rotational dynamics for the GdL complex.[3,28] Fig. 8 shows the ^1H NMRD profiles for the complexes at 25 and 37 °C. These profiles are distinct from those of commercial polyaminocarboxylate complexes, which begin to drop off at ~1 MHz and continue to drop with increasing field strength. This difference is important because clinical MRI experiments are performed at frequencies between 20 and 60 MHz,[29] a region where polyaminocarboxylate complexes reach a minimum in relaxivity, as opposed to HOPO-based complexes, which increase their relaxivity.

^1H NMRD profiles with such a relaxivity increase at high frequencies have been reported for polyaminocarboxylate ligands that are noncovalently bound to human serum albumin (HSA)[30] and specially in Gd^{3+} complexes of other HOPO derivatives.[31,32] As is known, the rotational correlation time (τ_R) is the main parameter that determines the effective correlation time of proton relaxation (τ_c) at magnetic fields relevant to MRI (30–60 MHz).[3c] Due to the relatively large number of parameters affecting relaxivity in Gd^{3+} complexes, it

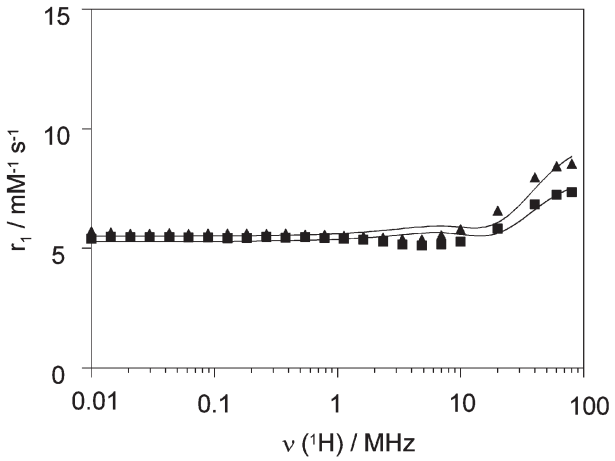

Fig. 8 NMRD profiles recorded for GdL complexes in aqueous solution, pH = 6.5, at different temperatures, 25 °C (■) and 37 °C (▲). The solid lines represent the least-squares fit as explained in the text.

is important to assess some of these parameters by independent measurements. Therefore, the self-diffusion coefficient of the complex, D_s^t, was determined by ^1H pulsed gradient spin echo (PGSE) NMR, on the diamagnetic La^{3+} analogue. The self-diffusion coefficient of LaL was measured at 298 K in D_2O, $D_s^t(D_2O) = (0.29 \pm 0.01) \times 10^{-9}$ m^2 s^{-1}. This self-diffusion coefficient depends on the solution viscosity η, the van der Waals radius of the complex, and a translational microviscosity factor f_s^t that accounts for the discrete nature of the solution through the Stokes–Einstein eqn (1) for translation.[33]

$$D_S^t = \frac{k_B T}{6\pi a f_S^t \eta} \quad (1)$$

From this equation, we can deduce the value of the self-diffusion coefficient in H_2O, which scales with the viscosity ratio $\eta(D_2O)/\eta(H_2O) = 1.24$, and is calculated to be $D_s^t(H_2O) = 0.36 \times 10^{-9}$ m^2 s^{-1}. The relative diffusion coefficient D can finally be deduced from the self-diffusion coefficient of H_2O, $D_s^t(H_2O) = 2.3 \times 10^{-9}$ m^2 s^{-1},[34] and is found to be $D(H_2O) = 2.66 \times 10^{-9}$ m^2 s^{-1}.

The Solomon–Bloembergen–Morgan theory was used for analyzing the experimental ^1H NMRD data.[35] In the analysis, we have fitted the rotational correlation time (τ_R^{298}), its activation energy (E_R) and the electron spin relaxation parameters (τ_V^{298}, Δ^2). The water exchange rate, the activation enthalpy and the relative diffusion constant have been fixed to the values determined above by ^{17}O NMR and by the ^1H pulsed gradient spin echo measurements, the Gd-water proton distance was fixed to $r_{GdH} = 3.1$ Å, and the distance of closest approach between the Gd^{3+} ion and the outer sphere protons to $a_{GdH} = 3.6$ Å.[36,37] The parameters obtained from the fitting of the data are shown in Table 4, and the corresponding fitted curves are shown in Fig. 7.

The value for the rotational correlation time obtained from the ^1H longitudinal relaxation rates ($\tau_R^{298} = 127$ ps) is characteristic of low molecular weight chelates, indicating that the

complex does not self-assemble in the concentration range studied. At high magnetic fields, the relaxivity is dominated by fast rotation in solution, as demonstrated by the temperature dependence of the relaxivity.

It should be emphasized that our fitted parameter for the rotational correlation time τ_R is in very good agreement with the values predicted from the Stokes–Einstein relation for the rotational diffusion constant (eqn (2)) of the complex.[33] Indeed, the rotational correlation time of a complex τ_R is defined as $\tau_R \equiv 1/6D_S^r$, with

$$D_S^r = \frac{k_B T}{8\pi a^3 f_S^r \eta} \quad (2)$$

where f_S^T is a microviscosity factor given by eqn (3)

$$f_S^r = \left[\frac{6a_w}{a} + \frac{1 + 3a_w/(a + 2a_w)}{(1 + 2a_w/a^3)}\right]^{-1} \quad (3)$$

a_w being the water molecule radius (a_w = 1.4 Å).

The volume of the GdL complex was estimated by means of DFT calculations on the corresponding La^{3+} analogue, and found to be 1011.1 Å^3. The radius (a) of the complex was then calculated to be a = 6.23 Å by considering a sphere having the same volume. This leads to a microviscosity factor f_S^T = 0.55, and a rotational correlation time τ_R = 135 ps, which is in excellent agreement with the fitted value. The value obtained is also consistent with other values reported for complexes of similar size.

The temperature and pH dependence of the 20 MHz r_1 relaxivity of the GdL complex are shown in Fig. S3 and S4,† respectively. As shown in Fig. S3,† in the range 2–50 °C, the value of r_1 decreases with the increase of the temperature, corresponding to a fast water exchange (k_{ex} (= $1/\tau_m$) > $1/T_{1M}$) and consequently to a short water exchange lifetime (τ_m). In these conditions, r_1 decreases due to the decrease of the rotational correlation time when the temperature increases. The pH study by proton relaxometry showed a common behaviour with other types of tripodal hydroxypyridinone-based compounds,[31,32] where for pH values between 2 and 3 the Gd^{3+} aquo-ion was the most abundant species, for pH values between 4 and 6 the relaxivity of the solution decreases steadily due to the decreasing presence of the Gd^{3+} aquo-ion and of Gd^{3+} complexes partially protonated at the pyridinone hydroxyl oxygens (GdH_3L and GdH_2L) with probable q values of 4 and 3, while for pH values between 6 and 8 the smaller relaxivity decrease results from the predominance of the complexes with q = 2, GdHL protonated at the apical nitrogen and the unprotonated GdL complex. This interpretation of the data is in qualitative agreement with the species distribution diagram for the La^{3+} complex (Fig. 5). Finally for pH > 8 the formation of Gd^{3+} hydroxide (or precipitation of GdL) leads to the observed abrupt decrease of r_1.

The kinetic stability of the [Gd–(NTP(PrHP)$_3$)] complex in solution towards transmetallation with Zn^{2+}, one of the most abundant endogenous metal ions with a concentration of ~32 μM in the human plasma,[38] was studied in a phosphate-buffered solution (10 mM, pH 7.1). If the transmetallation process occurs, the Gd^{3+} ions released due to their substitution in the complex by Zn^{2+} will precipitate as phosphate salt, and thus lead to a time-dependent decrease of the water proton longitudinal relaxation rate (R_1) of the solution containing an equimolar amount of Zn^{2+}, which is proportional to the amount of released Gd^{3+} ions.[39] In Fig. S5† the evolution with time of the ratio of paramagnetic relaxation rates $R_1^P(t)/R_1^P(0)$, where $R_1^P(t)$ and $R_1^P(0)$ are the paramagnetic relaxation rates at times t and zero, respectively, is shown for [Gd–(NTP(PrHP)$_3$)] in the presence of 10 mM phosphate buffer alone or also in the presence of Zn^{2+}. It can be concluded that there is only a very residual transmetallation process occurring in solution in the presence of an equimolar amount of Zn^{2+} and in the phosphate medium, which means that under *in vivo* conditions transmetallation with zinc should not occur. This complex is as stable in respect to transmetallation as those with macrocyclic ligands like $DOTA^{4-}$ or $HPDO3A^{3-}$ (DOTA = 1,4,7,10-tetraazacyclododecane-1,4,7,10-tetraacetate; HPDO3A = 2-[4-(2-hydroxypropyl)-7,10-bis(2-oxido-2-oxoethyl)-1,4,7,10-tetrazacyclododec-1-yl]acetate).[40]

2.4. Luminescent properties of [Ln–(NTP(PrHP)$_3$)] complexes

Experimental luminescence lifetimes of the Eu^{3+}, Tb^{3+}, Nd^{3+} and Yb^{3+}complexes with this ligand were recorded in H_2O and D_2O and analyzed in order to assess the hydration number (q) values. This is due to the differential quenching effect of the OH and OD oscillators of the bound H_2O and D_2O molecules, respectively,[41] although the calculation of the hydration number can also be carried out on the basis of second-sphere effects.[42] Measurements on the Tb^{3+} and Eu^{3+} complexes were surprisingly difficult to carry out due to the low intensities of the collected emission signals. For the Eu^{3+} complex, both lifetime values observed in H_2O and D_2O are low in comparison to the average ones observed for other Eu^{3+} complexes.[41,42] An explanation of this situation is the presence of a quenching process additional to the deactivation resulting from the overtones of water molecules bound to the lanthanide cation (that the empirical formula takes into account). More specifically, the quenching of a charge transfer energy state located at low energy is suspected here as Eu^{3+} can be reduced to Eu^{2+} and such electronic states have been documented to be efficient quenchers of the luminescence of Eu^{3+}.[43] Therefore, the use of the empirical formula to determine the q value for this Eu^{3+} complex is impossible as the formula cannot take into account the contribution of this additional quenching.

Measurements performed on the Tb^{3+} complex also resulted in the fitting of unreliable values of individual luminescence lifetimes in H_2O and D_2O, as the observed signal decay was not sufficiently intense to allow an accurate and reliable determination of the q value. This situation can be explained by a quenching of the excited states of Tb^{3+} that has been observed for several complexes: a Tb^{3+} to sensitizer back transfer.[44] This transfer results in the deactivation of the excited state of the lanthanide cation and shortens the luminescence lifetime at room temperature.

Attempts were then made to obtain q values by recording the luminescence lifetimes of the near-infrared (NIR) signals arising from Nd^{3+} and Yb^{3+} in their respective complexes. The average value of q = 0.5, calculated from the data obtained for the Yb^{3+} and Nd^{3+} complexes (0.6 and 0.4, respectively), is quite different from q = 2 evidenced by the ^{17}O chemical shifts, which is a strong indication that the determination of the q value based on NIR luminescence lifetimes of Nd^{3+} and Yb^{3+} for complexes in which the hydration is higher than 1 is unreliable. In fact, we have previously encountered a comparable situation with NIR emitting lanthanide complexes formed with another family of ligands where the correct value of 2 could be obtained from the Yb^{3+} complex but not from the corresponding Nd^{3+} complex.[45]

3. Conclusions

In summary, we have described the assessment and discussion of the most important physico-chemical parameters governing the properties of new lanthanide complexes with a tripodal hexadentate ligand containing three 3-hydroxy-4-pyridinone chelating units (tris-3,4-HOPO), in view of their potential application as medical diagnostic probes, in particular, the Gd^{3+} complexes as MRI contrast agents. Based on potentiometric determinations, this ligand forms mainly 1 : 1 Ln^{3+} complexes with high thermodynamic stability, despite some water-solubility limitations above pH *ca.* 7 due to deprotonation of the apical nitrogen and formation of a neutral complex species. The general trend of increasing log β_{MHL} with the reciprocal of the ionic radius (lanthanide contraction effect) was observed. Molecular modeling based on DFT calculations enabled an insight into the complex structure, indicating that the first coordination sphere of the lanthanides is occupied by the ligand (6 *O*-donor atoms) and two water molecules $[Ln(HL)(H_2O)_2]^+$ with the "out" conformation being more stable than the "in" conformation; furthermore, the calculated Gd–O (ligand) distances are in good agreement with the experimental data. Moreover, ^1H NMRD and ^{17}O NMR measurements showed the bishydrated nature of the GdL complex and a higher water proton relaxivity than the bench market low-molecular mononuclear compounds, although similar to other recently reported hydroxypyridinone based Gd chelates. The study of the luminescent properties of the complexes with NIR emitters was not conclusive, eventually because additional quenching to the non-radioactive effect was likely to take place (Eu^{3+} and Tb^{3+}) or unreliable values of q were produced (Nd^{3+} and Yb^{3+}). The Gd-induced relaxivity was not affected by the presence of Zn^{2+}, which was in accordance with the relatively lower stability of the Zn^{2+} complex as compared with that of the Gd^{3+} complex. This suggests that $NTP(PrHP)_3$ has a higher selectivity for Gd^{3+} coordination over competing Zn ions at cellular concentrations than that found for commercially available CAs. Thus, the combination of good thermodynamic stability with high relaxivity of the Gd-(tris-3,4-HOPO) chelate presented herein suggests promising gains in selectivity and sensitivity over the first generation of polyamino-carboxylate based CAs. Future developments on metallodrug analogues will be concerned with ligand extrafunctionalization to improve the bioavailability and the targeting of disease tissues or specific endogenous molecules, with further specificity/sensibility increase and toxicity decrease.

4. Experimental

4.1. Thermodynamic solution studies

Potentiometric titrations. The stock solution of HCl was prepared with doubly-distilled deionized water and standardized by titration with tris(hydroxymethyl)aminomethane (Aldrich). Potassium hydroxide solutions were prepared by dilution of a saturated solution and standardized with potassium hydrogen phthalate (Aldrich). The ionic strength of all solutions used in this study was adjusted to 0.1 mol dm^{-3} by appropriate amounts of 1 mol dm^{-3} KCl solutions. Stock solutions of lanthanide chlorides (50–100 mmol dm^{-3}) were prepared by reacting the appropriate oxide (Aldrich >99.9%) with 5.8–5.9 equivalents of hydrochloric acid (Aldrich >25%, PA). The solution slurry was mixed overnight and, if necessary, heated to minimize the undissolved solid. Excess of lanthanide oxide was filtered through a 0.2 μm syringe filter and the filtrate was diluted with 1–5 mmol dm^{-3} hydrochloric acid to the desired concentration. The stock solution of zinc (15.6 mmol dm^{-3}) was prepared by dilution of the appropriate salt ($ZnCl_2$). The lanthanide and zinc content in the stock solutions was determined by titration with EDTA and xylenol orange (Ln) or eriochrome black T (Zn) as an indicator; free acid concentrations in lanthanide solutions were checked by Gran's method.[46] Stock solutions thus prepared were subsequently used to prepare the diluted stock solutions employed to obtain the working solutions for the potentiometric and spectrophotometric measurements. A concentrated KCl solution (1 mol dm^{-3}) was used to adjust the ionic medium of these solutions.

The protonation constants of the ligand and the formation constants of its metal complexes were determined by potentiometric titrations. The temperature in the titration cell was maintained at 25.0 ± 0.1 °C by means of a circulatory bath. For all titrations, the electromotive force (emf) at the terminals of a combined glass electrode was measured and, before each titration, the glass electrode was calibrated to determine the hydrogen ion concentration following the reported procedure. A computer-controlled potentiometric apparatus collected emf data after each titrant addition, at intervals given by the data collection criterion, *i.e.* Δemf = 0.0 mV for 2 min: this condition was usually satisfied within 2–4 min in the calibration experiments, whereas a longer time was necessary to reach equilibrium in the experiments concerning ligand protonation and metal–ligand complexation (5–10 min). All measurements were carried out under an argon stream.

Potentiometric titrations of the ligand acid, alone or in the presence of metal ions, were carried out by adding standard

KOH to solutions of the ligand, containing an excess of mineral acid in the absence and presence of metal (Ln^{3+}, Zn^{2+}) ions. For the protonation study, titrations with three different ligand concentrations (C_L = 0.20, 0.59, 2.1 mmol dm^{-3}) were carried out. For the complexation study, three titrations for each system were carried out with ligand/M molar ratio ranging from ~1 to ~3 (details in ESI Table S2†). No solid phase was observed for the protonation study, while when Ln^{3+} ions were present a precipitate formed at $a = n_{OH}/n_{Ln^{3+}} \sim 7$. The protonation constants of the ligand and stability constants of the complexes were obtained by treating the experimental data with the Hyperquad program.[47]

UV-Vis measurements. Spectrophotometric titrations were carried out at 25.0 ± 0.1 °C on a Varian Cary 50 spectrophotometer, with optic fiber probes and a quartz cuvette with a 1 cm path length. The hydrogen ion concentration in the titration cell was measured, by a combined glass electrode calibrated as reported previously.[19] The pH in the solution cup was changed by small additions of standardized KOH and HCl. In the spectrophotometric experiments, the ligand concentration titration cell was $C_L = 1.3 \times 10^{-5}$ mol dm^{-3} and in the complexation study $C_{La} = 1.3 \times 10^{-5}$ mol dm^{-3} ($C_L/C_{La} = 1$). Due to the low concentration of the reagents, in this case formation of the solid phase did not occur even at very high pH (~11).

4.2. Molecular modeling studies

The structures of the complexes $[Ln(HL)(H_2O)_2]^+$ (Ln = La, Gd, Lu) were optimized by density functional theory (DFT) calculations using the program Gaussian09.[48] The B3LYP functional[49] was employed, since it has been often demonstrated to be suitable for predicting geometries of complexes with various metal ions, namely ferric complexes with the same ligand[15] as well as lanthanide complexes with other ligands.[50] The Stuttgart–Dresden small core potential for lanthanides was employed.[51] The other elements were treated using a Gaussian type 6-31G(d) basis set. Solvent effects were taken into account by the IEF-PCM method,[52] using the UFF radii for the spheres centred on each atom of the solute. The energies in the solvent were calculated using the gas-phase equilibrium geometry without further optimization.

4.3. Diffusion coefficient measurement

The diffusion coefficient of the diamagnetic LaL complex (1.0 mM, pD = 6.5) was measured in D_2O on a 500 MHz Bruker Avance 500 spectrometer by applying the bipolar stimulated spin-echo sequence to protons in the complex.[53] The proton gyromagnetic ratio is denoted by γ_I, the strength of the gradient pulse by g, the duration of this gradient by δ and the diffusion delay by Δ. The self-diffusion coefficient D_X^t of a species X was calculated by fitting of the theoretical expression of the proton signal intensity $I(\delta, \Delta, g) = I_0 \exp[-(\gamma_I g\delta)^2(\Delta - \delta/3) D_X^t]$, in which $I(\delta, \Delta, g)$ and I_0 are the intensities in the presence and absence of the gradient pulses, respectively. The values chosen for δ and Δ in these measurements depend on the magnitude of the diffusion coefficient being measured. For quickly diffusing HOD molecules, the values of δ and Δ were 1 and 100 ms respectively. For the slowly diffusing complex, they were 2 and 200 ms respectively. In the experiments, g was increased from 1.8 to 35.3 G cm^{-1}.

4.4. Variable temperature ^{17}O NMR measurements

Sample preparation. The GdL complex was prepared by mixing $GdCl_3$ and the ligand. A slight excess (5%) of ligand was used and the pH of the stock solution was adjusted by adding aqueous NaOH (0.1 mM). The solution was allowed to react for 24 h at 333 K. The absence of free metal was checked in each sample by testing with xylenol orange.[37,54]

The transverse ^{17}O relaxation rates ($1/T_2$) and the chemical shifts were measured in aqueous solution in the temperature range 278–348 K, on a Bruker Avance 500 (11.7 T, 67.8 MHz) spectrometer. The temperature was calculated according to previous calibration with ethylene glycol and methanol.[55] An acidified water solution ($HClO_4$, pH 3.3) was used as the external reference. Transverse relaxation times (T_2) were obtained by the Carr–Purcell–Meiboom–Gill spin-echo technique.[56] The technique of the ^{17}O NMR measurements on Gd^{3+} complexes has been described elsewhere.[57] The samples were sealed in glass spheres fitted into 10 mm NMR tubes to avoid susceptibility corrections of the chemical shifts.[58,59] To improve the sensitivity, ^{17}O-enriched water (10% $H_2{}^{17}O$, CortecNet) was added to the solutions to reach around 1% enrichment. The concentration of GdL, checked by the method of bulk magnetic susceptibility measurements, was 2.0 mM (pH = 6.5).

NMRD measurements. The measurements were performed on a 1 mM GdL solution by using a Stelar Spinmaster FFC NMR relaxometer (0.01–20 MHz) equipped with a VTC90 temperature control unit. At higher fields, the ^1H relaxivity measurements were performed on a Bruker electromagnet at frequencies of 20 MHz, 40 MHz, 60 MHz and 80 MHz. In each case, the temperature was measured by a substitution technique. Variable temperature measurements were performed at 25 and 37 °C. The ^{17}O NMR and ^1H NMRD data have been treated according to the Solomon–Bloembergen–Morgan theory of paramagnetic relaxation (see ESI†). The least-squares fit of the ^1H NMRD and ^{17}O NMR data was performed using Micromath Scientist version 2.0 (Salt Lake City, UT, USA). The reported errors correspond to two times the standard deviation.

Transmetallation studies with Zn^{2+}. The transmetallation reaction of the [Gd-(NTP(PrHP)$_3$)] complex with Zn^{2+} was studied by the time dependent decrease of the water proton longitudinal relaxation rate, R_1, measured on a Bruker Minispec mq20 (20 MHz, 25, 37 °C), of a phosphate-buffered saline solution (PBS, pH 6.7, 10 mM) containing 0.75 mM of the [Gd–L] complex after addition of an equimolar amount of $ZnCl_2$, while the sample was vigorously stirred.[39] The water longitudinal relaxation rate was also measured as a function of time on the PBS buffered solution (pH 6.7, 10 mM) containing 0.75 mM of the [Gd–L] complex.[40]

4.5. Luminescence lifetime measurements

Lanthanide-centered luminescence lifetimes were measured at 298 K using a Quantel YG 980 (266 nm, fourth harmonic) as the excitation source. Emission was collected at a right angle to the excitation beam and wavelengths were selected using interferential filters (1) 990 nm, BP20 for Yb^{3+}; 543 nm, BP22 for Tb^{3+}. Visible signals were monitored with the help of a Hamamatsu R928 photomultiplier tube and NIR signals were collected with a Hamamatsu H10330-45 detector. Resulting signals were collected on a 500 MHz band pass digital oscilloscope (Tektronix TDS 724C). Experimental luminescence decay curves containing 50 000 data points were treated with Origin 8.0 software using exponential fitting models. Three decay curves were collected on each sample ($C_{Ln} = C_L = 0.1$ mM, pH = 6.5 in H_2O and D_2O solution) and reported lifetimes are an average of at least three successful independent measurements.

Acknowledgements

This work was financially supported by Fundação para a Ciência e a Tecnologia, Portugal: projects PEst-OE/QUI/UI0100/2011, PTDC/QUI/70063/2006, grants SFRH/BPD/29874/2006 (S.M.M.) and SFRH/BD/46370/2008 (A.F.M.). AM acknowledges the Italian consortium CINECA (ISCRA Project HM2012) for the computing time. Financial support was received from La Ligue Contre le Cancer, France (E.T. and S.P.). The European COST D38 "Metal Based Systems for Molecular Imaging" and COST TD1004 "Theragnostics Imaging and Therapy" Actions are gratefully acknowledged.

References

1 V. W. W. Yam and K. K. W. Lo, *Coord. Chem. Rev.*, 1999, **184**, 157–240.
2 (*a*) L. Armelao, S. Quici, F. Barigelletti, G. Accorsi, G. Bottarod, M. Cavazzini and E. Tondello, *Coord. Chem. Rev.*, 2010, **254**, 487–505; (*b*) S. V. Eliseeva and J.-C. G. Bünzli, *Chem. Soc. Rev.*, 2010, **39**, 189–227.
3 (*a*) P. Caravan, J. J. Ellison, T. J. McMurry and R. B. Lauffer, *Chem. Rev.*, 1999, **99**, 2293–2352; (*b*) P. Caravan, N. J. Cloutier, M. T. Greenfield, S. A. McDermid, S. U. Dunham, M. Bulte, J. C. Amedio Jr., R. J. Looby, R. M. Supkowski, W. DeW Horrocks Jr., T. J. McMurry and R. B. Lauffer, *J. Am. Chem. Soc.*, 2002, **124**, 3152–3162; (*c*) P. H. Fries, D. Imbert and A. Melchior, *J. Chem. Phys.*, 2010, **132**, 044502.
4 R. S. Ranganathan, N. Raju, H. Fan, X. Zhang, M. F. Tweedle, J. F. Desreux and V. Jacques, *Inorg. Chem.*, 2002, **41**, 6856–66.
5 D. D. Castelli, E. Gianolio, S. G. Crich, E. Terreno and S. Aime, *Coord. Chem. Rev.*, 2008, **252**, 2424–2443.
6 T. Storry, K. H. Thompson and C. Orvig, *Chem. Soc. Rev.*, 2006, **35**, 534–544.
7 (*a*) S. Aime, S. G. Crich, E. Gianolio, G. B. Giovenzana, L. Tei and E. Terreno, *Coord. Chem. Rev.*, 2006, **250**, 1562–1579; (*b*) C. F. G. C. Geraldes and S. Laurent, *Contrast Media Mol. Imaging*, 2009, **4**, 1–23.
8 K. N. Raymond and V. C. Pierre, *Bioconjugate Chem.*, 2005, **16**, 3–8.
9 E. J. Werner, A. Datta, C. J. Jocher and K. N. Raymond, *Angew. Chem., Int. Ed.*, 2008, **47**, 8568–8580.
10 E. J. Werner, S. Avedano, M. Botta, B. P. Hay, E. G. Moore, S. Aime and K. N. Raymond, *J. Am. Chem. Soc.*, 2007, **129**, 1870–1871.
11 A. Datta and K. N. Raymond, *Acc. Chem. Res.*, 2009, **42**, 938–947.
12 D. Parker, *Chem. Soc. Rev.*, 2004, **33**, 156–165.
13 E. G. Moore, A. P. S. Samuel and K. N. Raymond, *Acc. Chem. Res.*, 2009, **42**, 542–552.
14 C. J. Jocher, E. G. Moore, J. D. Pierce and K. N. Raymond, *Inorg. Chem.*, 2008, **46**, 7951–7953.
15 S. Chaves, S. M. Marques, A. M. F. Matos, A. Nunes, L. Gano, T. Tuccinardo, A. Martinelli and M. A. Santos, *Chem.–Eur. J.*, 2010, **16**, 10535–10545.
16 S. Chaves, S. M. Marques, A. C. Mendonça, A. F. Martins, M. I. M. Prata, A. C. Santos, C. F. G. C. Geraldes and M. A. Santos, *J. Inorg. Biochem.*, 2011, **105**, 31–38.
17 H. S. Thomsen, *Radiol. Clin. North Am.*, 2009, **47**, 827–831.
18 R. M. Smith and A. E. Martell, in *Critical Stability Constants*, Plenum Press, New York, 1989.
19 D. Guo, C. Y. Duan, F. Lu, Y. Hasegawa, Q. J. Meng and S. Yanagida, *Chem. Commun.*, 2004, 1486–1487.
20 P. Di Bernardo, P. L. Zanonato, A. Bismondo, A. Melchior and M. Tolazzi, *Dalton Trans.*, 2009, 4236–4244.
21 P. Di Bernardo, A. Melchior, M. Tolazzi and P. L. Zanonato, *Coord. Chem. Rev.*, 2012, **256**, 328–351.
22 E. N. Rizkalla, *Radiochim. Acta*, 1993, **61**, 181–189.
23 P. Di Bernardo, P. L. Zanonato, A. Melchior, R. Portanova, M. Tolazzi, G. R. Choppin and Z. Wang, *Inorg. Chem.*, 2008, **47**, 1155–1164.
24 J. Xu, S. J. Franklin, D. W. Whisenhunt Jr. and K. N. Raymond, *J. Am. Chem. Soc.*, 1995, **117**, 7245–7246.
25 S. M. Cohen, J. Xu, E. Radkov, K. N. Raymond, M. Botta, A. Barge and S. Aime, *Inorg. Chem.*, 2000, **39**, 5747–5756.
26 G. Xiao, D. Helm, R. C. Hider and P. S. Dobbin, *Inorg. Chem.*, 1995, **34**, 1268–1270.
27 M. K. Thompson, M. Botta, G. Nicolle, L. Helm, S. Aime, A. E. Merbach and K. N. Raymond, *J. Am. Chem. Soc.*, 2003, **125**, 14274–14275.
28 S. Aime, M. Botta, M. Fasano and E. Terreno, *Chem. Soc. Rev.*, 1998, **27**, 19–29.
29 M. F. Tweedle, in *Relaxation Agents in NMR Imaging*, ed. J.-C. G. Bunzli and G. R. Choppin, Elsevier, Amsterdam, 1989, pp. 127–179.
30 S. Aime, M. Botta, M. Fasano, S. Geninatti Crich and E. Terreno, *Coord. Chem. Rev.*, 1999, **321**, 185–186.
31 C. P. Valérie, M. Botta, S. Aime and K. N. Raymond, *Inorg. Chem.*, 2006, **45**, 8355–8364.

32 C. P. Valérie, M. Botta, S. Aime and K. N. Raymond, *J. Am. Chem. Soc.*, 2006, **128**, 5344–5345.
33 S. Rast and P. H. Fries, *J. Chem. Phys.*, 2000, **113**, 8724–8735.
34 M. Holz and H. Weingärtner, *J. Magn. Reson.*, 1991, **92**, 115–125.
35 A. E. Merbach and E. Toth, *Chichester in The Chemistry of Contrast Agents in Medical Magnetic Resonance Imaging*, Wiley, 2001.
36 M. F. Ferreira, A. F. Martins, J. A. Martins, P. M. Ferreira, E. Toth and C. F. G. C. Geraldes, *Chem. Commun.*, 2009, 6475–6477.
37 D. H. Powell, O. M. NiDhubhghaill, D. Pubanz, L. Helm, Y. S. Lebedev, W. Schlaepfer and A. E. Merbach, *J. Am. Chem. Soc.*, 1996, **118**, 9333–9346.
38 L. S. Nikolaeva, V. V. Chirkov, N. A. Dobrynina, L. A. Lyapina and V. E. Pastorova, *Pharm. Chem. J.*, 2005, **39**, 57–63.
39 S. Laurent, L. V. Elst, F. Copoix and R. N. Muller, *Invest. Radiol.*, 2001, **36**, 115–122.
40 S. Laurent, L. V. Elst, A. Vroman and R. N. Muller, *Helv. Chim. Acta*, 2007, **90**, 562–573.
41 (*a*) W. DeW Horrocks Jr. and D. R. Sudnick, *J. Am. Chem. Soc.*, 1979, **101**, 334–340; (*b*) R. M. Supkowski and W. DeW Horrocks Jr., *Inorg. Chem.*, 1999, **38**, 5616–5619.
42 A. Beeby, I. M. Clarkson, R. S. Dickins, S. Faulkner, D. Parker, L. Royle, A. S. de Sousa, J. A. G. Williams and M. Woods, *J. Chem. Soc., Perkin Trans. 2*, 1999, 493–504.
43 S. Petoud, J.-C. G. Bünzli, T. Glanzman, C. Piguet, Q. Xiang and R. P. Thummel, *J. Luminesc.*, 1999, **82**, 69–79.
44 J.-C. G. Bünzli and C. Piguet, *Chem. Soc. Rev.*, 2005, **34**, 1048–1077.
45 F. Caillé, C. S. Bonnet, F. Buron, S. Villette, L. Helm, S. Petoud, F. Suzenet and É. Tóth, *Inorg. Chem.*, 2012, **51**, 2522–2532.
46 G. Gran, *Analyst*, 1952, **77**, 661–671.
47 P. Gans, A. Sabatini and A. Vacca, *Talanta*, 1996, **43**, 1739–1753.
48 M. J. Frisch, G. W. Trucks, H. B. Schlegel, G. E. Scuseria, M. A. Robb, J. R. Cheeseman, G. Scalmani, V. Barone, B. Mennucci, G. A. Petersson, H. Nakatsuji, M. Caricato, X. Li, H. P. Hratchian, A. F. Izmaylov, J. Bloino, G. Zheng, J. L. Sonnenberg, M. Hada, M. Ehara, K. Toyota, R. Fukuda, J. Hasegawa, M. Ishida, T. Nakajima, Y. Honda, O. Kitao, H. Nakai, T. Vreven, J. A. Montgomery, J. E. Peralta, F. Ogliaro, M. Bearpark, J. J. Heyd, E. Brothers, K. N. Kudin, V. N. Staroverov, R. Kobayashi, J. Normand, K. Raghavachari, A. Rendell, J. C. Burant, S. S. Iyengar, J. Tomasi, M. Cossi, N. Rega, J. M. Millam, M. Klene, J. E. Knox, J. B. Cross, V. Bakken, C. Adamo, J. Jaramillo, R. Gomperts, R. E. Stratmann, O. Yazyev, A. J. Austin, R. Cammi, C. Pomelli, J. W. Ochterski, R. L. Martin, K. Morokuma, V. G. Zakrzewski, G. A. Voth, P. Salvador, J. J. Dannenberg, S. Dapprich, A. D. Daniels, Ö. Farkas, J. B. Foresman, J. V. Ortiz, J. Cioslowski and D. J. Fox, *Revision A.02*, Gaussian, Inc., Wallingford CT, 2009.
49 (*a*) A. D. Becke, *J. Chem. Phys.*, 1993, **98**, 1372–1377; (*b*) C. T. Lee, W. T. Yang and R. G. Parr, *Phys. Rev. B: Condens. Matter*, 1988, **37**, 785–789.
50 (*a*) A. Melchior, E. S. Marcos, R. R. Pappalardo and J. M. Martínez, *Theor. Chem. Acc.*, 2011, **128**, 627–638; (*b*) U. Cosentino, A. Villa, D. Pitea, G. Moro, V. Barone and A. Maiocchi, *J. Am. Chem. Soc.*, 2002, **124**, 4901–4909.
51 X. Y. Cao and M. Dolg, *J. Chem. Phys.*, 2001, **115**(16), 7348–7355.
52 B. Mennucci and J. Tomasi, *J. Chem. Phys.*, 1997, **106**, 5151–5158.
53 A. Jerschow and N. Müller, *J. Magn. Reson.*, 1997, **125**, 372–375.
54 R. Hovland, A. J. Aasen and J. Klaveness, *Org. Biomol. Chem.*, 2003, **1**, 1707–1710.
55 D. S. Raiford, C. L. Fisk and E. D. Becker, *Anal. Chem.*, 1979, **51**, 2050–2051.
56 S. Meiboom and D. Gill, *Rev. Sci. Instrum.*, 1958, **29**, 688–691.
57 K. Micskei, L. Helm, E. Brucher and A. E. Merbach, *Inorg. Chem.*, 1993, **32**, 3844–3850.
58 A. D. Hugi, L. Helm and A. E. Merbach, *Helv. Chim. Acta*, 1985, **68**, 508–521.
59 S. C. Chu, Y. Xu and J. A. Balschi, *Magn. Reson. Med.*, 1990, **13**, 239–262.